한국항해항만학회지 제48권 제5호
J. Navig. Port Res. Vol. 48, No. 5 : 349-359, October 2024 (ISSN:1598-5725(Print)/ISSN:2093-8470(Online))
DOI : http://dx.doi.org/10.5394/KINPR.2024.48.5.349

A Study of Maneuverability Prediction of Air Cushion Vehicles Using Virtual Captive Model Test Results

Thi Thanh Diep Nguyen · Thi Loan Mai** · Hoang Thien Vu*** · Hyeon Kyu Yoon**** · † Jongyeol Park*

**Researcher, Industrial Technology Research Center, Changwon National University, Korea*
***Researcher, Sungshin Defence Solution, Korea*
****Student, Department of Naval Architecture and Marine Engineering, Changwon National University, Korea*
*****, † Professor, Department of Smart Ocean Mobility Engineering, Changwon National University, Korea*

Abstract : *The maneuverability of an Air Cushion Vehicle (ACV) is a critical aspect of its performance, affecting its stability, control, and overall operational effectiveness. Despite the operational complexity due to the interaction of aerodynamic and hydrodynamic forces, significant strides have been made in predicting its maneuverability. This paper discusses the maneuverability prediction of ACV based on virtual captive model tests. Hydrodynamic and aerodynamic forces on ACV's were assessed through computational fluid dynamics (CFD) calculations. Subsequently, a maneuvering simulation considering these forces was performed. The paper explores the results of aerodynamic and hydrodynamic forces during static tests such as static drift and circular motion tests. Additionally, the maneuverability performance in turning and zig-zag tests was evaluated. Furthermore, these performances were compared with the maneuvering standards suggested by the International Maritime Organization (IMO). The outcomes from the virtual captive model tests have significantly enhanced the predictive accuracy of ACV maneuverability, contributing to refined design and operational strategies.*

Key words : *air cushion vehicles (ACV), hydrodynamic forces, aerodynamic forces, maneuverability, computational fluid dynamics*

1. Introduction

An air cushion Vehicle (ACV), commonly known as a hovercraft, is unique in its ability to traverse various terrains, including water, land, ice, and mud. This versatility makes it invaluable in both military and civilian applications, ranging from amphibious assaults and search-and-rescue missions to commercial transportation and recreational use. However, the inherent complexity of its operation, driven by an interaction of aerodynamic and hydrodynamic forces, poses significant challenges in predicting its maneuverability.

Traditional experimental methods for evaluating ACV maneuverability, such as full-scale trials and scaled physical model tests, are often constrained by high costs, logistical challenges, and the difficulty of replicating diverse environmental conditions. To overcome these limitations, maneuvering simulation using the virtual captive model test results has emerged as a promising alternative. The virtual captive model tests involve the use of sophisticated computer simulations to create a virtual environment that closely mimics real-world conditions. By capturing intricate dynamics of ACV in this controlled setting, the virtual captive model test can provide detailed insights into ACV maneuverability characteristics under various scenarios. This approach not only enhances predictive accuracy but also allows for extensive testing without practical constraints associated with physical trials. A virtual captive model test is usually used to obtain the aerodynamic and hydrodynamic forces due to the low cost and convenience of replicating diverse environmental conditions (Tabaczek et al., 2009; Aram and Silva, 2019; Yang et al., 2022; Muhammad et al., 2023; Nguyen et al., 2022). In addition, aerodynamic forces considered as wind forces can be estimated in various ways. Fujiwara et al. (1998) provided a simpler method to estimate wind forces and moment acting on the ship hull. The stepwise method is used by linear multiple regression analysis. Furthermore, Fujiwara et al. (2005) presented a new method to calculate wind forces based on the wind loads and physical components acting on the hull's ship. In this study, wind forces consisted of cross and longitudinal flow drags with induced and lift drags.

† Corresponding author, jyp@changwon.ac.kr 055)213-3688
* nguyenthithanhdiep1994@gmail.com 055)213-2930
** mailoankttt@gmail.com 055)213-2930
*** vuhoangthienpm@gmail.com 055)213-2930
**** hkyoon@changwon.ac.kr 055)213-3683

Wind moments were calculated by crossing the lateral wind force to the moment lever. Momoki et al. (2009) conducted an experiment in a wind tunnel for a full-scale model test and measured wind forces and moment acting on the superstructure of a model. A computational fluid dynamics (CFD) program was then developed to investigate the wind flow characteristics around the superstructure. Ueno et al. (2012) investigated wind load coefficients in various ship types and loading conditions using eight parameters of the ship's principal dimensions. The most acceptable parameter that gives better estimates of wind forces than other parameters was ship breadth. Janssen et al. (2017) conducted a simulation to calculate wind forces on a container ship using 3D steady RANS CFD. Results of wave forces were validated with wind forces obtained by wind-turbine measurement and the impact analysis of geometrical simplifications. Xiong and Zhang (2017) performed a three-dimensional numerical calculation of the airflow around a container ship. The airflow around the superstructure of a container ship was evaluated using the flow pattern around it and the wind load acting on it.

The maneuverability of an ACV is a critical aspect of its performance, influencing its stability, control, and overall operational effectiveness. The predicting ship maneuvering performance is usually focused on turning and course-keeping abilities using the hydrodynamic obtained from experiments, empirical formulas, or numerical methods for common ships (Koo et al., 2013; Nguyen et al., 2021; Kim and Kim, 2021; Choi et al., 2023). However, the ACV has unique operational characteristics in maneuvering performance. Lu et al. (2019) conducted the experiment and numerical on the resistance and motion of the ACV. In this study, the resistance was investigated due to the influence of the cushion compartment. Zhao et al. (2003) performed a turning circle performance simulation of an ACV in three degrees of freedom. In addition, the turning circle tests were carried out in various wind directions. Eremeyew et al. (2017) presented a dynamic mathematical model of an ACV to predict the resistance and vertical motion. In addition, an experiment was conducted to confirm the results of numerical calculation. Lu et al. (2010) investigated the course stability of an ACV in four degrees of freedom. A series of experiments was conducted using a horizontal planar motion mechanism to determine the hydrodynamic derivatives. However, the hydrodynamic derivatives were not shown in their paper. In general, there has not been a virtually comprehensive analysis of hydrodynamic forces and maneuverability such as turning and course-keeping abilities of the ACV investigated.

In this study, the maneuverability prediction of an ACV was investigated using the results of aerodynamic and hydrodynamic forces obtained from virtual captive model tests through CFD calculation. Static drift and circular motion tests were conducted to obtain hydrodynamic forces acting on the ACV hull. In addition, static drift tests in various drift angles are carried out to estimate aerodynamic forces. Turning and zig-zag tests were conducted to evaluate the maneuverability of the ACV.

2. Maneuvering simulation

2.1 Target ship

In this study, the maneuverability of an ACV was predicted. The hull was composed of a skirt and a structure above the skirt. The principal particulars of the ACV are listed in Table 1. A 3D modeling of the ACV is shown in Fig. 1. The target ACV was modeled with two thrusters at the bow and two propellers and deflectable rudders at the stern. In addition, project areas of the ACV in various directions were estimated.

Table 1 Principal particulars

Item	Unit	Value
Length, L	m	21.000
Breadth, B	m	8.000
Depth, D	m	0.572
Speed, U	knots	30.000
Displacement, Δ	ton	35.000
Transverse project area, A_T	m^2	33.860
Lateral project area, A_L	m^2	92.520
Skirt length, L_S	m	21.000
Skirt breadth, B_S	m	8.000
Skirt width, W_S	m	1.000

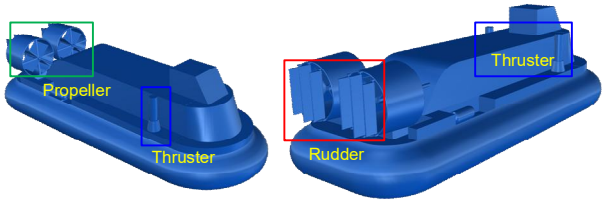

Fig. 1 3D modeling of ACV

2.2 Virtual captive model test

The hydrodynamic and aerodynamic forces were calculated by conducting a series of virtual captive model tests using a commercial CFD program of ANSYS-FLUENT. The test conditions of the CFD calculation to obtain hydrodynamic and aerodynamic forces are listed in Table 2. Governing equations were applied in momentum and continuity equations with an assumption of an incompressible flow. Boundary domain sizes followed ITTC recommendations for CFD calculation (ITTC, 2014). Boundary conditions such as inlet, outlet, top, bottom and sides are set following the physical characteristics as shown in Fig. 2.

Table 2 Virtual captive model test conditions

Type of force	Type of test	Variables
Hydrodynamic	Static drift	drift angle: 0°~180° (interval 10°)
	Circular motion	non-dimensionalized yaw rate: 0.2 ~0.6 (interval 0.1)
Aerodynamic	Static drift	drift angle: 0°~180° (interval 10°)

In CFD calculation, a shear stress transport ($k-\omega$ SST) turbulence model is usually used to predict aerodynamic and hydrodynamic forces due to some advantages in time calculation and accuracy. When calculating hydrodynamic forces, the open channel flow and the volume of the fluid are applied to determine the free surface and two flow phases of the air and water. When calculating aerodynamic forces, only the flow phase of the air is defined. The pressure is adjusted to ensure satisfied continuity of the velocity field using a semi-implicit method for the pressure-linked equation (SIMPLE) to solve the governing equation. The gradient of the flow variable is evaluated using the least square cell-based method. Fig. 3 shows details of the meshing during CFD calculation. The mesh quality was checked with the mesh metrics spectrum suggested by ANSYS before performing the calculation. The grid number is about 7.9 million. In addition, mesh skewness and orthogonal quality, which represent the degree to which a mesh cell deviates from an ideal shape and the orthogonality of mesh cell faces to the flow direction or adjacent cells, are commonly used to assess mesh quality. Mesh skewness and orthogonal quality are 0.83 and 0.17, respectively. According to the mesh quality recommendations suggested by ANSYS, the mesh quality was acceptable for calculation (Adam et al., 2020).

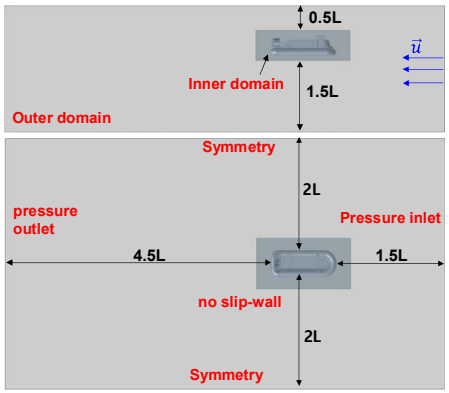

(a) For calculating hydrodynamic forces

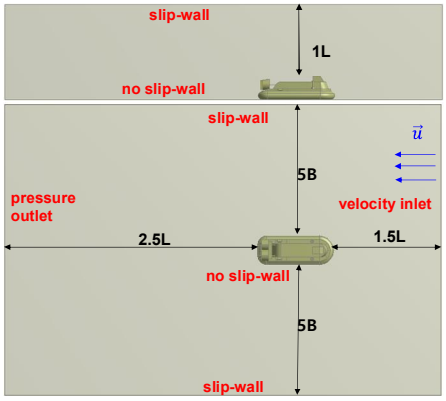

(b) For calculating aerodynamic forces

Fig. 2 Boundary domain

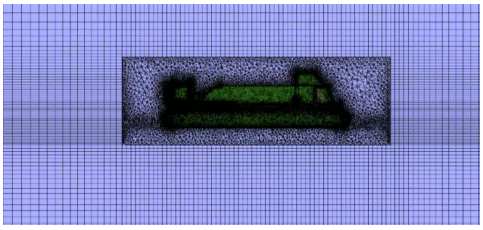

(a) For calculating hydrodynamic forces

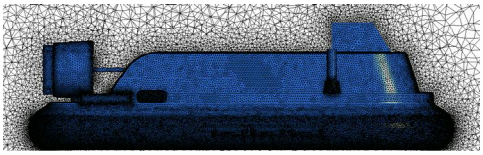

(b) For calculating aerodynamic forces

Fig. 3 Meshing in CFD calculation

2.3 Mathematical model

2.3.1 Coordinate system

The maneuverability of an ACV is investigated in four degrees of freedom due to the influence of aerodynamic forces. The coordinate system of the ACV maneuvering is determined based on the earth-fixed $Ox_0y_0z_0$ and ship-fixed $O_sx_sy_sz_s$ frame as shown in Fig. 4. The earth-fixed coordinate $Ox_0y_0z_0$ is defined by the right-hand Cartesian axis x_0, y_0, and z_0, and the origin O located at the water surface. In addition, ship-fixed O_s is located at the midship. X and Y denote surge and sway forces, respectively. K and N represent roll and yaw moment, respectively. U, u, and v are ship speed, surge and sway velocities, respectively. p and r are angular velocities.

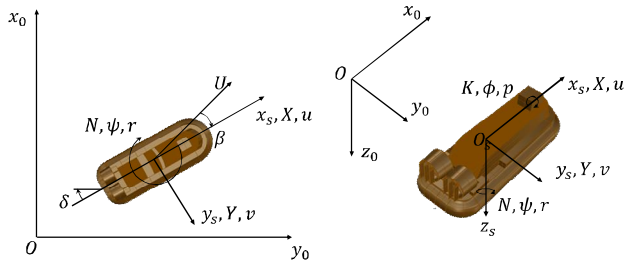

Fig. 4 Definition of the coordinate system

2.3.2 Equation of motion

The maneuvering mathematical model of ACV is examined by four degrees of freedom. Hence, surge and sway forces and roll and yaw moments are considered. The mathematical model can be written following surge, sway, roll, and yaw motion as shown in Eq. (1). m, I_x, I_z, and I_{zx} are the mass and inertia moments of ACV, respectively. x_G and z_G are longitudinal and vertical center of gravity of ACV, respectively. $\dot{p}$ and $\dot{r}$ denote angular accelerations.

$$\begin{aligned} X &= m(\dot{u} - vr - x_G r^2 + z_G rp) \\ Y &= m(\dot{v} + ur - z_G \dot{p} + x_G \dot{r}) \\ K &= I_x \dot{p} - I_{zx} \dot{r} - mz_G(\dot{v} - ur) \\ N &= I_z \dot{r} - I_{zx} \dot{p} + mx_G(\dot{v} + ur) \end{aligned} \tag{1}$$

The effect of the cushion is treated as a force acting on the hull. Even if air escapes from the gap formed under the skirt during heeling, the static pressure inside the skirt is maintained. The vertical weight and buoyancy are always in equilibrium. The added mass due to contact between the skirt and the water surface is negligible compared to its mass. External forces acting on the ACV hull consist of forces acting on the hull, propeller, thruster, and rudder forces, as shown in Eq. (2).

$$\begin{aligned} X &= X_H + X_P + X_T + X_R \\ Y &= Y_H + Y_T + Y_R \\ K &= K_H + K_T + K_R \\ N &= N_H + N_P + N_T + N_R \end{aligned} \tag{2}$$

Hydrodynamic forces acting on the ACV hull can be classified into hydrodynamic, aerodynamic, restoring, and skirt cushion forces. The mathematical model of hydrodynamic forces acting on ACV hull is modeled as described in Eq. (3). The hydrodynamic and aerodynamic forces are obtained by CFD calculation. Eqs. (4)-(5) express aerodynamic and hydrodynamic forces acting on the ACV hull, respectively. In addition, hydrodynamic forces and moments are non-dimensionalized by $0.5\rho LdU^2$ and $0.5\rho L^2 dU^2$, respectively. The surge, sway, roll, and yaw forces in aerodynamic forces are non-dimensionalized $0.5\rho_A A_T U^2$, $0.5\rho_A A_L U^2$, $0.5\rho_A A_L^2 U^2/L$, and $0.5\rho_A A_L L U^2$, respectively. ρ, ρ_A, L, d, and U represent water density, air density, length, draft, and speed of the ship, respectively. A_T and A_L are traversal and lateral project areas of the ACV, respectively.

$$\begin{aligned} X_H &= X_H^A + X_H^H \\ Y_H &= Y_H^A + Y_H^H + Y_H^C \\ K_H &= K_H^A + K_H^H + K_H^R + K_H^C \\ N_H &= N_H^A + N_H^H \end{aligned} \tag{3}$$

$$\begin{aligned} X_H^A &= X_{vv}^A v^2 + X_{vvvv}^A v^4 \\ Y_H^A &= Y_v^A v + Y_{v|v|}^A v \mid v \mid \\ K_H^A &= K_v^A Uv + K_{v|v|}^A v \mid v \mid + K_p^A Up \\ N_H^A &= N_v^A v + N_{v|v|}^A v \mid v \mid \end{aligned} \tag{4}$$

$$\begin{aligned} X_H^H &= X_{u|u|}^H u|u| + X_{vvvv}^H v^4 + X_{vv}^H v^2 + X_{rr}^H r^2 \\ Y_H^H &= Y_v^H v + Y_{v|v|}^H v|v| + Y_r^H r + Y_{r|r|}^H r|r| \\ K_H^H &= K_p^H Up + K_v^H v + K_{v|v|}^H v|v| + K_r^H r + K_{r|r|}^H r|r| \\ N_H^H &= N_v^H v + N_{v|v|}^H v|v| + N_r^H r + N_{r|r|}^H r|r| \end{aligned} \tag{5}$$

The roll restoring moment generated by buoyance and gravity is given as Eq. (6), where g, GM, and ϕ are gravity acceleration, transverse metacentric height, and roll angle, respectively. Forces due to skirt cushion occur when ACV heels and a gap form between the skirt and the water surface, resulting in a change in momentum as air escapes. In addition, the draft of ACV is affected by the pressure of the skirt cushion. When the pressure of the skirt cushion is less than the hull mass, the draft of ACV is calculated

using the following Eq. (7). P_C and A_C denote pressure and pressure area of skirt, respectively. L_S, B_S, and W_S are length, breadth, and width of the skirt cushion, respectively. S_S represents the water area in contact with the skirt as annular. Forces due to the cushion are determined with Eq. (8), where C_C and z_C are the contraction coefficient and vertical position of the skirt, respectively.

$$K_H^R = -mgGM\phi \tag{6}$$

$$d = \frac{mg - P_C A_C}{\rho_w g S_S} \tag{7}$$

where, $A_C = L_S B_S - S_S$ and $S_S = 2(L_S + B_S - 2W_S)W_S$

$$\begin{aligned} Y_H^C &= C_C A_C P_C \tan\phi \\ K_H^C &= -Y_H^C z_C \end{aligned} \tag{8}$$

Forces due to the propeller are written as Eq. (9), where ρ_A, n, and D_P denote air density, propeller revolution, and propeller diameter, respectively. K_T is a function of the advanced ratio of the propeller J. In addition, the forces of the thruster at the bow are described in Eq. (10), where V_j and Q denote the thruster jet speed and volumetric flow rate of air ejected by the bow thruster, respectively. x_T, y_T, and z_T are longitudinal, lateral, and vertical positions of the bow thruster, respectively. The rudder forces and moments are affected significantly by the interaction between the ship hull and the rudder, and the behind propeller flow when the rudder is deflected. Similar to the conventional ship, the velocity in the propeller race is calculated by the approximation formula available from momentum theory (Van Mannen and Van Oossanen, 1989). In this case, the propeller is assumed as a thin disk that imparts the momentum of the fluid that passes through it. Based on this theory, the outflow velocity aft of the propeller, which will be denoted as the velocity at the rudder U_R can be determined as Eq. (11) by the inflow velocity U_A and the function of the advanced ratio. F_N is the rudder's normal force. δ, A_R, and f_α represent rudder angle, rudder area and rudder lift gradient coefficient, respectively. x_R, y_R, and z_R are the longitudinal, lateral, and vertical positions of the rudder, respectively. In addition, forces and moments due to the rudder are expressed in Eq. (13) (Lewandowski, 2003).

$$\begin{aligned} X_P &= \rho_A D_P^4 K_T n|n| \\ N_P &= -y_P X_P \end{aligned} \tag{9}$$

$$\begin{aligned} X_T &= -\rho_A V_j Q \cos\psi_T \\ Y_T &= \rho_A V_j Q \sin\psi_T \\ K_T &= -z_T Y_T \\ N_T &= x_T Y_T - y_T X_T \end{aligned} \tag{10}$$

$$U_R = U_A \sqrt{1 + \frac{8K_T}{\pi J^2}} \tag{11}$$

$$F_N = \frac{1}{2}\rho_A A_R u_R^2 f_\alpha \sin\delta \tag{12}$$

$$\begin{aligned} X_R &= -F_N \sin\delta \\ Y_R &= F_N \cos\delta \\ K_R &= -z_R Y_R \\ N_R &= x_R Y_R - y_R X_R \end{aligned} \tag{13}$$

3. Results

3.1 Hydrodynamic and aerodynamic forces

Hydrodynamic and aerodynamic forces are calculated by a series of virtual captive model tests. Hydrodynamic forces are investigated in various drift angles and yaw rates by performing static drift and circular motion tests. Fig. 5 shows the results of hydrodynamic forces in various drift angles. Hydrodynamic forces change significantly in various drift angles due to changes in water resistance and flow dynamics around the hull. Surge force is primarily influenced by the hull's resistance to forward motion. The surge force is dominant at drift angles of nearly 45° and 135° while it decreases when the drift angle approaches 0° and 180°, especially at a drift angle of 90°. The sway force is the smallest at drift angles of 0° and 180° because the vehicle moves straight ahead without lateral deviation. The largest sway force is dominant due to a strong lateral displacement when the drift angle approaches 90°. Roll and yaw moments are minimal at drift angles of 0° and 180° as there is a symmetrical water flow on both sides of the hull. In the oblique drift angle, roll and yaw moments become substantial, risking the ACV's balance, which could potentially cause severe rotational motion. In this case, corrective measures are needed to prevent capsizing because controlling the ship's direction is difficult without robust steering mechanisms.

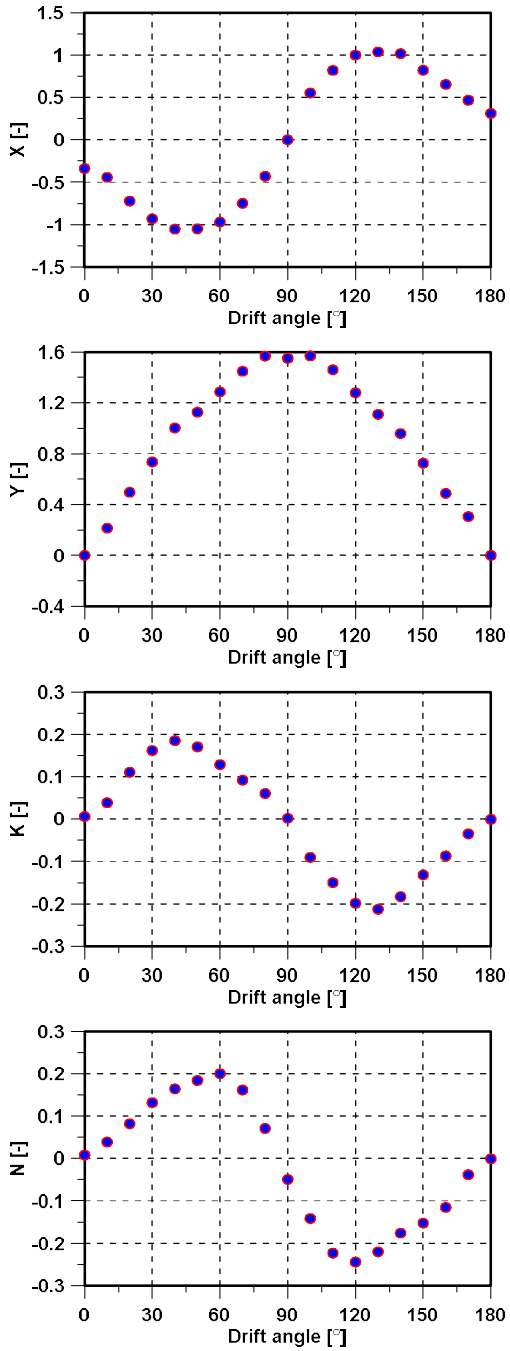

Fig. 5 Hydrodynamic forces at various drift angles

Fig. 6 shows the results of hydrodynamic forces at various yaw rates. Hydrodynamic forces change significantly in various yaw rates due to changes in dynamics around the hull's rotational motion. In general, hydrodynamic forces increase dramatically with an increase in yaw rate, especially in the case of sway force and moments. With a high yaw rate, the sway force becomes more significant, pushing the vehicle laterally as the water flow becomes more uneven. Moments start to appear due to slight asymmetric forces on either side.

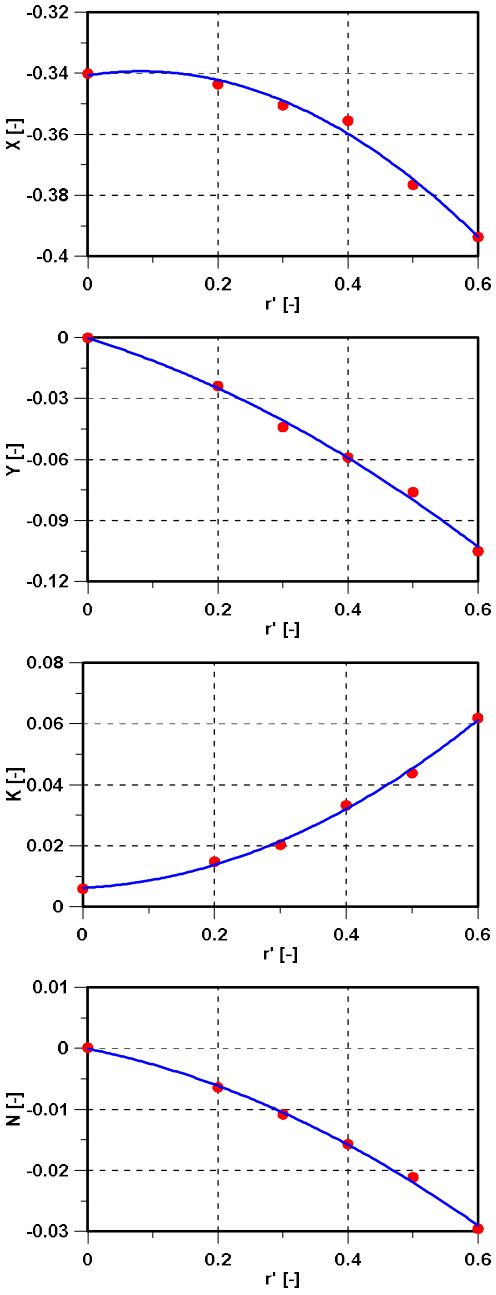

Fig. 6 Hydrodynamic forces at various yaw rates

Fig. 7 shows the results of the aerodynamic forces at various drift angles. As in the same case of hydrodynamic forces, aerodynamic forces change significantly at various drift angles due to changes in air flow around the hull. Surge force is primarily affected by headwind resistance and propulsion efficiency. It is at its minimum with the largest lateral project area at a drift angle of 90° while sway force reaches the largest value. The roll moment shows the same trend as the sway force. It is the smallest when the drift angle approaches 0° and 180°. In addition, the yaw moment is minimal at drift angles of 0° and 180°

as there is a symmetrical airflow on both sides of the hull. Yaw moment increases significantly at drift angles of nearly 45° and 135°. Results of hydrodynamic and aerodynamic coefficients obtained in the virtual captive model test are listed in Table 3.

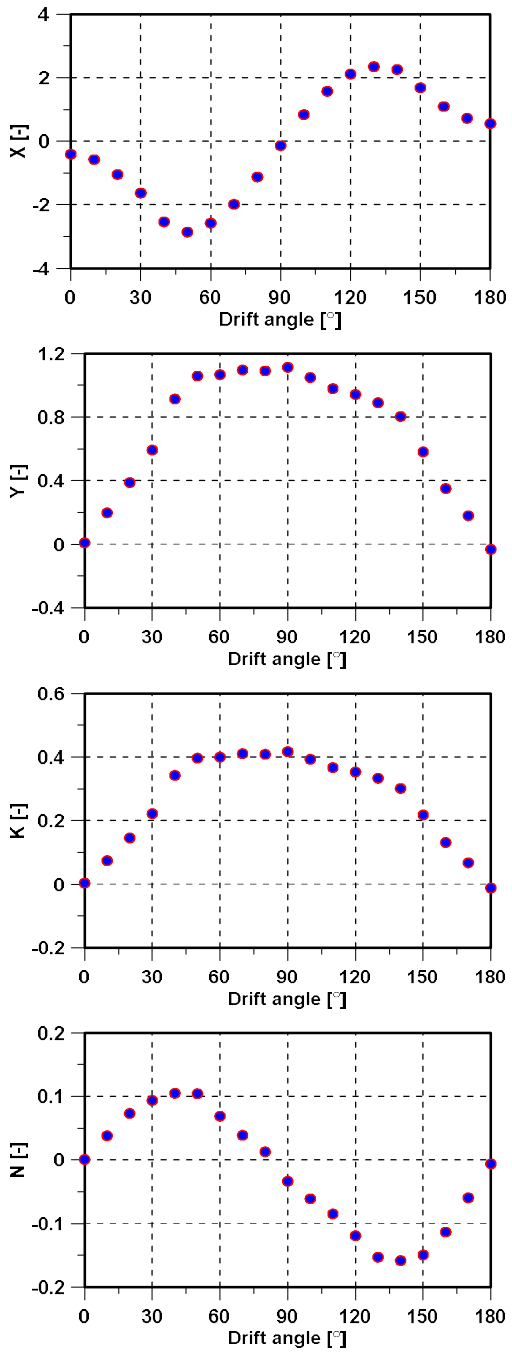

Fig. 7 Aerodynamic forces at various drift angles

Table 3 Hydrodynamic coefficients

Coefficient	Value	Coefficient	Value
$X^H_{u\|u\|}$	-3.00E-01	$K^H_{v\|v\|}$	-3.51E-02
X^H_{vv}	-2.80E-01	K^H_{p}	-3.00E-02
X^H_{vvvv}	2.73E-02	K^H_{r}	-4.52E-01
X^H_{rr}	-2.52E-01	$K^H_{r\|r\|}$	-9.27E-01
X^A_{vv}	-7.59E-01	K^A_{v}	-4.51E-01
X^A_{vvvv}	-5.90E-02	$K^A_{v\|v\|}$	-4.81E-02
Y^H_{v}	-7.14E-01	K^A_{p}	-1.00E-02
$Y^H_{v\|v\|}$	-6.85E-02	N^H_{v}	-2.72E-02
Y^H_{r}	-3.01E-02	$N^H_{v\|v\|}$	2.20E-02
$Y^H_{r\|r\|}$	-3.18E-02	N^H_{r}	-2.59E-02
Y^A_{v}	-8.10E-01	$N^H_{r\|r\|}$	-2.10E-03
$Y^A_{v\|v\|}$	-2.28E-01	N^A_{v}	-3.15E-02
K^H_{v}	-4.77E-01	$N^A_{v\|v\|}$	2.56E-02

3.2 Turning and zigzag tests

The maneuvering simulations are conducted for the turning circle and the zig-zag tests. The influence of rudder deflection and skirt pressure are investigated to evaluate the turning ability of the ACV. In order to investigate the effect of rudder deflection, the turning tests are performed at rudder angles (δ) of 10°, 20°, 30°, and 35° at the target skirt's pressure P_C of 1830 Pa. Results of the turning circle tests such as ACV trajectories, surge and sway velocities, and roll and yaw rates in various rudder angles are shown in Fig. 8. The turning circle changes dramatically due to a change of rudder angle. The tactical diameter is the largest for the smallest steering angle, indicating a wider turn. It is the smallest for the largest steering angle, indicating a sharper turn. This shows that the ACV can achieve tighter turns at larger rudder angles. The ACV's maneuverability improves with larger steering angles, allowing for tighter turns and greater control in confined spaces. However, this comes at the cost of higher lateral forces, which may affect stability, as shown in sway velocity and roll and yaw rates. Tactical diameters at δ of 10°, 20°, 30°, and 35° are 8.698L, 5.966L, 4.937L, and 4.674 L, respectively. Furthermore, advances at δ = 10°, 20°, 30°, and 35° are 8.598L, 6.288L, 5.146L, and 4.990L, respectively. Results of the turning circle tests are listed in Table 4.

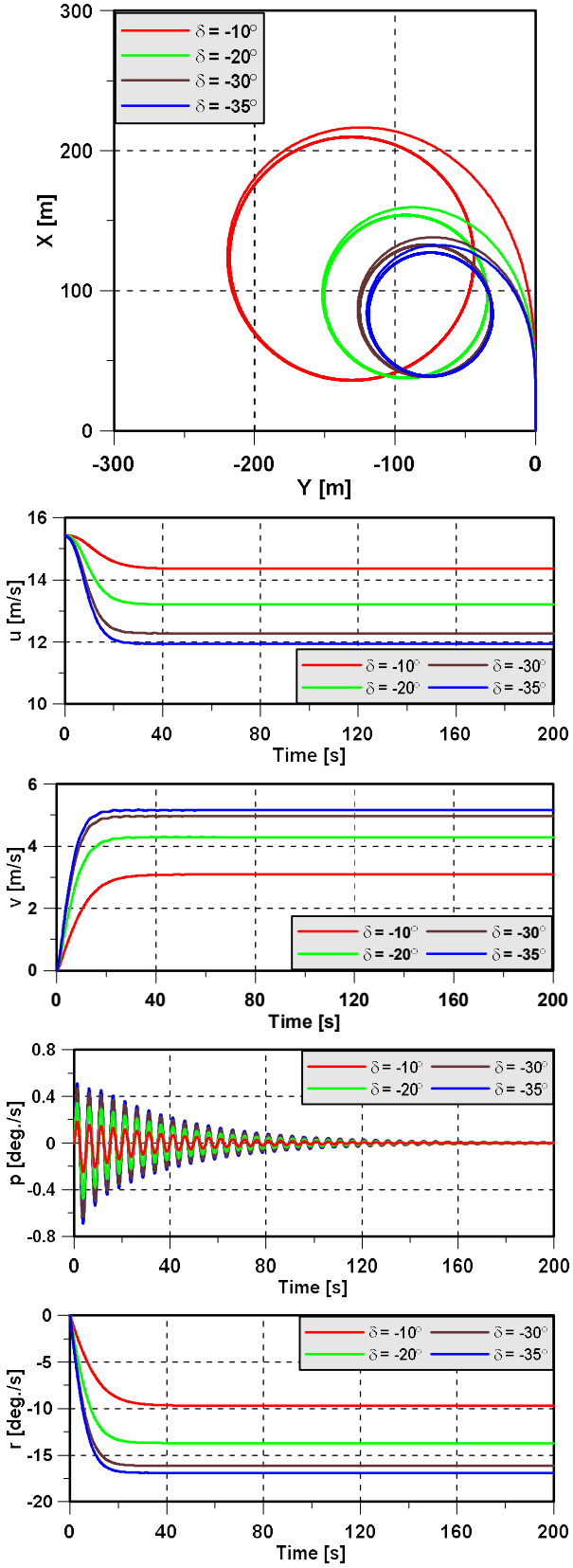

Fig. 8 Results of the turning circle test

Table 4 Result of turning circle test

Item	Advance [Lpp]	Tactical diameter [Lpp]
δ = 10°	8.598	8.698
δ = 20°	6.288	5.966
δ = 30°	5.146	4.937
δ = 35°	4.990	4.674
IMO standard (δ = 35°)	4.500	5.000

The effect of the skirt's pressure is investigated in the turning tests. The varied parameters due to the changing of the skirt's pressure in this simulation are listed in Table 5. Fig. 9 shows the comparison of the turning trajectory in various skirt's pressures. When the skirt's pressure increases, the draft is reduced as the vehicle rises due to the skirt's pressure. In the same velocity condition, the lower draft causes the lower revolution rate of the propeller due to the lower hydrodynamic forces. The turning radius is significantly reduced as the pressure increases due to the lower hydrodynamic forces. The turning radius could also be decreased with additional control forces by the thrusters at the bow.

Table 5 Parameters in various skirt's pressure

Item	P_{C_1}	P_{C_2}	P_{C_3}	P_{C_4}	P_C
Skirt pressure [Pa]	500.0	1000.0	1500.0	2000.0	1830.0
Draft [m]	0.527	0.422	0.317	0.212	0.248
Propeller revolution [rpm]	2168.4	1956.6	1696.0	1387.3	1500.0
Ship speed [knots]	30.0				

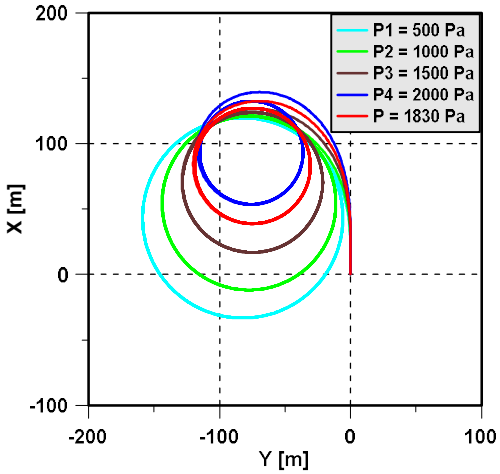

Fig. 9 Turning trajectory according to the skirt's pressure

In addition, 10°/10° zig-zag and 20°/20° zig-zag tests are performed to investigate course-keeping and yaw-checking abilities. Figs. 10-11 show the results of ACV's 10°/10° zig-zag and 20°/20° zig-zag tests. In the 10°/10° zig-zag test, characteristics related to 1st and 2nd overshoot angle (OSA) are evaluated. The 1st and 2nd OSA are 7.950° and 17.188°, respectively. While the time to 1st and 2nd OSA are 9.520 s and 24.680 s, respectively. Furthermore, characteristics of 1st OSA is checked in the 20°/20° zig-zag test. The 1st OSA and time to 1st OSA are 14.388° and 9.62 s, respectively. Results of the zig-zag test are listed in Table 6.

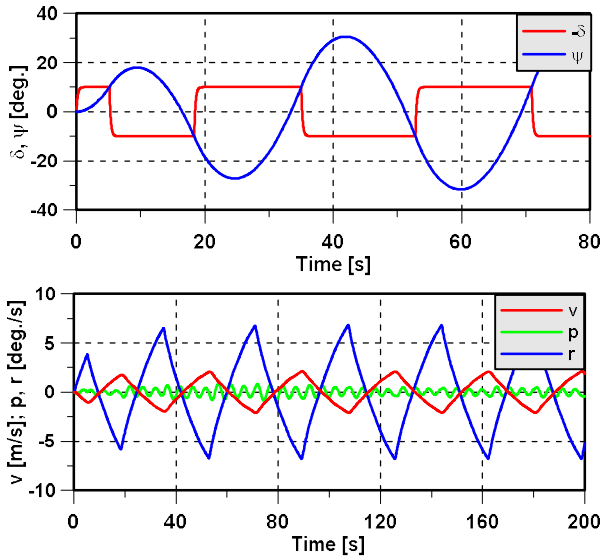

Fig. 10 Results of the 10°/10° zig-zag test

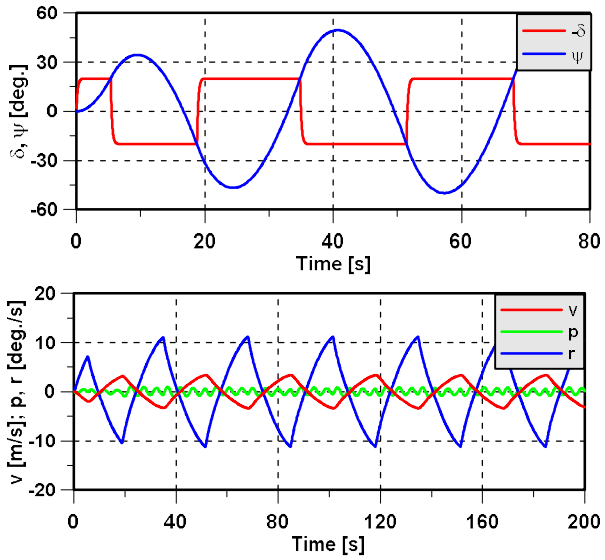

Fig. 11 Results of the 20°/20° zig-zag test

Table 6 Result of zig-zag test

Item	Zig-zag test		IMO standard	
	10°/10°	20°/20°	10°/10°	20°/20°
1st OSA	7.950	14.388	10	25
Time to 1st OSA	9.520	9.620	-	-
2nd OSA	17.188	-	25	-
Time to 2nd OSA	24.680	-	-	-

The results of the turning and zig-zag tests are compared with the criteria of ship maneuvering suggested by the International Maritime Organization (IMO, 2002). The criteria for turning tests for advance and tactical diameter are $4.5L$ and $5.0L$, respectively. The advance is a bit larger than the criteria, however, the tactical diameter satisfies the criteria. The 1st and 2nd OSA of the 10°/10° zig-zag meet the criteria of the zig-zag test of 10° and 25°, respectively. The 1st OSA of the 20°/20° zig-zag is smaller than the criteria of the zig-zag test of 25°.

4. Conclusions

This paper investigated ACV maneuverability using CFD calculation results. It has the following conclusions:

Hydrodynamic and aerodynamic forces were obtained by performing a series of virtual captive model tests in various drift angles and yaw rates. The change in drift angle and yaw rate significantly affected hydrodynamic and aerodynamic forces.

A mathematical ACV maneuvering model was established to consider various components. When the external forces acting on the ACV's hull and components of aerodynamic forces, restoring forces, and skirt cushion forces are considered beside hydrodynamic forces in conventional ships.

Maneuverabilities of ACV were evaluated by conducting turning circle and zig-zag tests. The results of turning and zig-zag tests were compared with maneuvering criteria. All most characteristics of maneuverability satisfied the criteria.

Acknowledgements

This research was supported by Future Challenge Program through the Agency for Defense Development funded by the Defense Acquisition Program Administration.

References

[1] Adam, N. M., Attia, O. H., Sulttami, A. O. A., Mahmood, H. A., As'arry, A. and Rezali, K. A. M.(2020), "Numerical Analysis for Solar Panel Subjected with an External Force to Overcome Adhesive Force in Desert Areas", CFD letters, Vol. 12, No. 9, pp. 60-75.

[2] Aram, S. and Silva, K. M.(2019), "Computaional Fluid Dynamics Prediction of Hydrodynamic Derivatives for Maneuvering Models of a Fully-Appended Ship", Proceeding of the 17th International Ship Stability Workshop, Finland.

[3] Choi, H., Kwon, S. Y., Kim, S. H. and Kim, I.. T.(2023), "Study on the Manoeuvring Performance of a Fishing Vessel Based on CFD Simulation of the Hull Forms and Rudder Shapes", Journal of Ocean Engineering and Technology, Vol. 37, No. 4, pp. 129-136.

[4] Eremeyew, V. O., Penlin, F. S. and Tumanin, A. V.(2017), "Mathematical Model of Dynamics of Air Cushion Vehicle with Ballonet Type Skirt on Water", Procedia Engineering, Vol. 206, pp. 354-359.

[5] Fujiwara, T., Ueno, M. and Nimura, T.(1998), "Estimation of Wind Forces and Moments acting on Ships", Journal of Society of Naval Architects of Japan, Vol. 183, pp. 77-90.

[6] Fujiwara, T., Ueno, M. and Ikeda, Y.(2005), "A New Estimation Method of Wind Forces and Moments acting on Ships on the basis of Physical Component Models", Journal of the Japan Society of Naval Architects and Ocean Engineers, Vol. 2, pp. 243-255.

[7] International Maritime Organization (IMO).(2002), "Resolution MSC.137(76): Standard for Ship Manoeuvrability", pp. 1-8.

[8] ITTC - Recommended Procedures and Guidelines. (2014), "Practical Guidelines for Ship CFD Applications". 7.5-03-02-03, pp. 1-19.

[9] Janssen, W. D., Blocken, B. and Wijhe, H. J. V.(2017), "CFD Simulation of Wind Loads on a Container Ship: Validation and Impact of Geometrical Simplifications", Journal of Wind Engineering and Industrial Aerodynamics, Vol. 166, pp. 106-116.

[10] Kim, I. T. and Kim, S. H.(2021), "Numerical Study to Evaluate Course-Keeping Ability in Regular Wave Using Weather Vaning Simulation", Journal of Ocean Engineering and Technology, Vol. 35, No. 1, pp. 13-23.

[11] Koo, B., Lee, J. and Kang, D.(2013), "Study on Variation of Ship's Course Keeping Ability under Waves Depending on Rudder Type", Journal of Ocean Engineering and Technology, Vol. 27, No. 2, pp. 87-92.

[12] Lewandowski, E. M.(2003), "The Dynamics of Marine Craft: Maneuvering and Seakeeping", World Scientific Publishing, USA.

[13] Lu, J., Huang, G. L. and Li, S. Z.(2010), "Four-Degree-of-Freedom Course Stability of an Air Cushion Vehicle", Journal of Shanghai Jiaotong University, Vol. 15, No. 2, pp. 163-167.

[14] Lu, S., Zou, J., Zhang, Y. and Guo, Z.(2019), "Experimental and Numerical Study on Motion and Resistance Characteristics of the Partial Air Cushion Supported Catamaran", Water 2019, Vol. 11, No. 5, pp. 1-24.

[15] Momoki, T., Onishi, S., Katayama, T. and Ikeda, Y.(2009), "A Study on Wind Pressure Characteristics of Ship with Large Superstructures", Proceedings of the 19th International Offshore and Polar Engineering Conference, Japan, pp. 563-569.

[16] Muhammad, A. H., Paroka, D., Rahman, S, Nikmatuallah, M. I. and Sudirman, L.(2023), "Hydrodynamic Derivatives of a Ferry Ship Maneuvering in Deep and Shallow Water with Computational Fluid Dynamic Method", IOP Conference Series: Earth and Environmental Science, Vol. 1198, pp. 1-10.

[17] Nguyen, T. T. D., Mai, V. T., Lee, S. and Yoon, H. K.(2022), "An Experiment Study on Hydrodynamic Forces of Korea Autonomous Surface Ship in Various Loading Conditions", Journal of Navigation and Port Research, Vol. 6, No. 2, pp. 73-81.

[18] Nguyen, V. M., Nguyen, T. T. D., Yoon, H. K. and Kim, Y. H.(2021), "Numerical Study on Unified Seakeeping and Maneuvering of a Russian Trawler in Wind and Waves", Journal of Ocean Engineering and Technology, Vol. 35, No. 3, pp. 173-182.

[19] Tabaczek, T., Gornicz, T. and Kulczyk, J.(2009), "CFD Based Hull Hydrodynamic Forces for Simulation of Ship Manoeuvres", International Journal on Marine Navigation and Safety of Sea Transportation, Vol. 3, No. 1, pp. 31-35.

[20] Ueno, M., Kitamura, F., Sogihnara, N. and Fujiwara, T.(2012), "A Simple Method to Estimate Wind Loads on Ships", the 2012 World Congress on Advance in Civil, Environmental and Materials Research, Korea,

pp. 2314-2322.

[21] Van Mannen, J. D. and Van Oossanen, P.(1989), “Principles of Naval Architecture” The Society of Naval Architects and Marine Engineers.

[22] Xiong, H. S. and Zhang, D. X.(2017), “Research on Wind Loads of Container Ship based on CFD”, Book: Current Trends in Computer Science and Mechanical Automation, Vol. 2, pp. 342-355.

[23] Yang, B., Kaidi, S. and Lefrancois, E.(2022), “CFD Method to Study Hydrodynamics Forces Acting on Ship Navigating in Confined Curved Channels with Current”, Journal of Marine Science and Engineering, Vol. 10, pp. 1-21.

[24] Zhao, S. Q., Shi, X. C., Shi, Y. L. and Bian, X. Q.(2003), “Simulation Study of Plane Motion of Air Cushion Vehicle”, Journal of Marine Science and Application, Vol. 2, No. 2, pp. 67-71.

Received 04 October 2024
Revised 10 October 2024
Accepted 24 October 2024